Self-organization of cellular magnetic-domain patterns

Per Bak
Department of Physics, Brookhaven National Laboratory, Upton, New York 11973

Henrik Flyvbjerg
The Niels Bohr Institute, Blegdamsvej 17, DK-2100 Copenhagen Ø, Denmark
(Received 22 August 1991)

We model the self-organizing dynamics of two-dimensional magnetic-domain patterns. Using a random-neighbor approximation, avalanches of topological rearrangements and domain destruction are easily simulated numerically, and asymptotic forms for distributions of avalanche sizes and lifetimes can be given analytically. Recent experimental results for such distributions are found to obey these asymptotic forms, which permits us to classify the self-organized state observed in experiments as subcritical.

PACS number(s): 05.40.+j, 75.10.Nr, 75.60.−d

I. INTRODUCTION

Figure 1 shows a digitized photograph of a small part of a magnetic garnet film. The film is biased with an external magnetic field H_B pointing out of the plane. The black lines joining at threefold vertices are narrow domains of down magnetization. The white areas are domain of up magnetization. A number of experiments with domain formation and growth in such films are described by Westervelt and co-workers in Refs. [1–3]. In Ref. [3] it was observed that over a significant interval of applied magnetic field and domain sizes the system self-organizes into barely stable configurations. When in this state, small increments in the external field would trigger avalanchelike processes of topological rearrangements and cell destruction spanning two orders of magnitude in size and lifetime. The experimental distributions of avalanche sizes and lifetimes appeared to follow power laws, and it was suggested that the system might have organized itself into a critical state, thus constituting an example of self-organized criticality [4].

In the present article we describe the dynamical properties of these domain patterns with a random-neighbor model (Secs. II and III). In Ref. [5], this model was found to describe the coarsening dynamics of two-dimensional domain patterns well. Here we find that the domain pattern self-organizes to a *subcritical* state. Our model's avalanches of topological rearrangements and cell destruction obey power laws with mean-field exponents and exponential damping factors (Secs. IV and V). We reanalyze the experimental results of [3] in terms of such distributions and find they fit with χ^2 confidence levels of 99.8% for avalanche sizes and 99.7% for avalanche lifetimes. These unrealistically high levels indicate that the error bars on the experimental results were overestimated. Even if the experimental errors are reduced by a factor of 2, we still find χ^2 levels above 70% for the distributions mentioned (Sec. VI). We discuss sources of errors in our model and ways to improve the model. Finally, we conclude that the statistical properties of the avalanches of topological rearrangements found in two-dimensional magnetic-domain patterns with pentagonal bubble traps are well described by assuming self-organization of the domain patterns to a subcritical state (Sec. VII).

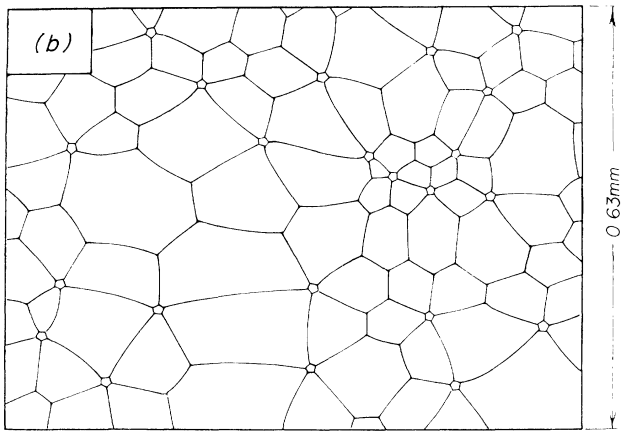

FIG. 1. Digitized photograph of a magnetic-domain pattern. This is Fig. 8(b) from Ref. [2].

II. KINEMATICS AND DYNAMICS

With reference to Fig. 1 and similar patterns, we shall refer to domains of up magnetization as simply *domains* and to a stripe of down magnetization separating two such domains as a domain *wall*. The *topological number* n—or, shorter, the *topology* of a domain—is the number of walls forming its boundary. It is also equal to the number of 3-vertices in its boundary. We make this trivial observation here, because it is the latter definition which is generalized to more complicated networks of domain walls below.

We only consider domain patterns with external bias field $H_B > H_{\mathrm{RI}}$ where H_{RI} is the run-in field value. In this range the tension τ in domain walls is positive [1,2]. Consequently, the kinematics and dynamics of the domain pattern resemble that of an ideal soap froth in

two dimensions. In particular, the tension in the walls gives rise to a force on any part of a wall, perpendicular to it, and inversely proportional in strength to the local radius of curvature of the wall. A coercive drag acting on any part of the wall gives it a finite mobility σ in response to this force [1], while vertices are mere geometrical points having infinite mobility. The net result is curvature-driven dynamics, resulting in domain walls that are arcs of circles, joining at 120° angles at 3-vertices. This dynamics is also found for ideal soap froths in two dimensions [6].

As a consequence of this dynamics, one has von Neumann's law for the rate of change of the area A_n of any domain—or soap bubble—with topology n [7]:

$$\frac{dA_n}{dt}=\frac{\pi}{3}\sigma\tau(n-6)\ . \tag{1}$$

Here σ is the permeability of the walls in the case of soap froths and the wall mobility in the case discussed here. According to this law, all domains with more than six neighbors increase their area with time and those with exactly six are static, while those with less than six shrink and eventually disappear from the ensemble of domains when their areas vanish. Because the average topology is six as a consequence of Euler's law, Eq. (1) conserves the total area $A=\sum_n A_n$, while the average area grows, since domains disappear from the pattern.

For $H_B\in[H_{\rm RI},H_5]=$ [83.5 Oe, 98.5 Oe], Westervelt and co-workers found that domains with $n=5$ would shrink only to a certain small size determined by the value of H_B and then remain static [1,2,3]. This behavior violates von Neumann's law, not just for these *pentagonal bubble traps,* which should not exist, but also for their neighbor domains, whose areas should feed on the shrinking pentagons and whose topologies should change when a pentagon vanishes. Since the pentagonal bubble traps have much smaller areas than other domains in the pattern (see Fig. 1), we may choose to neglect their areas and treat them as effective 5-vertices. They are also to a good approximation fivefold symmetric; i.e., the five walls joined by a trap meet at 72° angles. If for a moment we assume this to be rigorously true, we can copy von Neumann's derivation of his law [7] and obtain the following generalization of it: The rate of change of the area $A_{n,m}$ of a domain with a boundary containing n 3-vertices and m 5-vertices is

$$\frac{dA_{n,m}}{dt}=\frac{\pi}{15}\sigma\tau(5n+9m-30)\ . \tag{2}$$

Here σ and τ are the wall mobility and tension, as before. According to Eq. (2), any domain having $n+2m\leq 6$ will shrink, with the exception of domains with $(n,m)=(6,0)$, which remain static. We should bear in mind, however, that we have assumed that 5-vertices are symmetric with 72° angles between the walls they join. This is a strong assumption: While a 3-vertex can remain static only if the three walls joined by it are separated by 120° angles, there is a two-parameter family of angles between walls joined by a 5-vertex that will leave a 5-vertex static. Since $A_{4,1}$, $A_{2,2}$, and $A_{0,3}$ will remain static, if their 5-vertices join their walls at 60° angles, and because the difference between 60° and 72° is small, one might expect the pattern to relax to configurations making Eq. (2) invalid.

Fortunately, we do not need von Neumann's law or its generalization Eq. (2) for the line of arguments presented below. Their qualitative contents suffice: We shall speak only of 3-vertices and assume the following.

(1) Any domain with topology $n<5$ shrinks and disappears from the ensemble of domains when its area vanishes.

(2) Any domain with $n=5$ shrinks until its area reaches trap size, whereupon it remains in the ensemble with static area.

(3) Except that two or more bubble traps cannot be neighbors, such a configuration is unstable, and if it is created by the dynamics, the neighbor traps disappear together from the ensemble.

The third assumption is motivated by the observation in [1,2] that pentagonal bubble traps can be destabilized by a sufficiently strong local field from a sufficiently high local density of domain boundaries. This nonlocal interaction between domain boundaries is too complicated for us to model in detail, but two or more neighboring domains with small area certainly represent a high local density of domain boundaries—actually a divergent density for vanishing area—so we expect the third assumption to catch essential features of the actual mechanism of destabilization of pentagonal bubble traps. It is certainly in accord with the photographs in [1,2,3], none of which have pentagonal bubble traps next to each other for $H_B>H_{\rm RI}$.

We have not specified the area of the pentagonal bubble traps, except as being small. One may think of it as being zero and of our description as a coarse-grained one, but nowhere below do we really need their area to be zero.

As a consequence of Euler's law for the plane and the fact that we have only 3-vertices in the network of domain walls, we have a topological conservation law in addition to the three assumptions above: when a domain with n neighbors vanishes, its *topological deficit* $6-n$ is transferred to its neighbors, so that the average number of neighbors in the ensemble remains six. For example, when a domain with three neighbors disappears its three neighbors each loses a neighbor [see Fig. 2(a)]. The deficit, $6-n=3$ is conserved. Similarly, when an isolated pentagonal trap disappears, two of its neighbors each loses a neighbor and one gains one [see Fig. 2(b)]. Again, the deficit $6-n=1$ is conserved.

Since pentagons do not necessarily disappear from the pattern, but can remain in it as traps, the pattern may end up in a static configuration, from which all domains with four or fewer neighbors have vanished and all domains with five neighbors have become traps. Such a configuration is static, because no domains can shrink, and hence no domains can grow.

We use the three assumptions above, the conservation of local topological deficit, and a random-neighbor approximation, which was found quite accurate for curvature-driven domain growth in two dimensions [5].

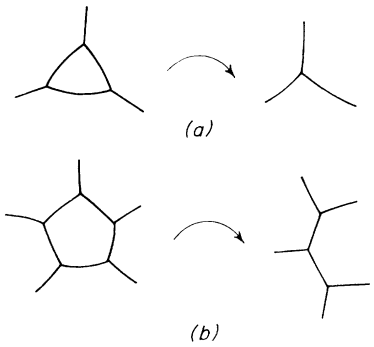

FIG. 2. Domain with n neighbors disappears, and its neighbors lose a total of $6-n$ neighbors. (a) $n=3$. (b) $n=5$. Note that two neighbors each lose a neighbor, while one gains a neighbor.

The basic idea behind this approximation is the observation that, while there may be very definite rules, such as von Neumann's law, determining the dynamics of the individual domain in a pattern, *correlations* between domains are weak. Even correlations between nearest-neighbor domains are small: They manifest themselves, for example in Aboav's law, which gives the average topology $\overline{m}(n)$ of domains neighboring domains with topology n [8,6]:

$$\overline{m}(n)=6-a+\frac{6a+\mu_2}{n} . \tag{3}$$

Here a is a free parameter believed to be determined by the dynamics driving the domain growth, and μ_2 is the second moment of the relative frequency P_n of domains with topology n:

$$\sum_n P_n=1 \quad \text{(normalization)} , \tag{4}$$

$$\sum_n nP_n=6 \quad \text{(Euler)} , \tag{5}$$

$$\sum_n (n-6)^2P_n=\mu_2 \quad \text{(definition of } \mu_2) . \tag{6}$$

Babcock, Seshadri, and Westervelt found $a=1.2$ $\mu_2=0.83$ at $H_B=89$ Oe, which is in the middle of the interval $[H_{\mathrm{RI}},H_5]$ [2]. In our random-neighbor approximation, on the other hand, we assume that at any wall in the network of domain boundaries, one finds a domain with topology n with probability proportional to P_n *and* also proportional to n, the number of walls in such a domain. The resulting normalized probability for the topology n of a domain found at a random wall is

$$Q_n\equiv\frac{n}{6}P_n . \tag{7}$$

Thus, for any value of n,

$$\overline{m}(n)=\sum_m mQ_m=\tfrac{1}{6}\sum_m m^2P_m=6+\frac{\mu_2}{6} , \tag{8}$$

in the random-neighbor approximation. This result is identical to Eq. (3) for $n=6$. We use it only for $n=5$, where it differs by only 4% from Eq. (3). In general, for most patterns, P_n differs significantly from zero only for n near 6, i.e., where Eq. (8) is a good approximation to Eq. (3). This justifies the random-neighbor approximation, provided μ_2 is not changed much by the approximation.

III. STEADY-STATE DYNAMICS

Let us examine a static configuration of the domain pattern: The ensemble of domains can contain no domains with topology $n<5$, since such domains cannot be static, but will shrink and disappear. The only domains having $n=5$ are bubble traps, since domains with this topology and larger area will shrink, yielding their area to their neighbors. No bubble traps are neighbors, since such a constellation is unstable by assumption. Domains having $n\geq 6$ are static either by von Neumann's law (case of $n=6$) or because there are no shrinking domains and, hence, no growing ones. In short, any configuration is static if and only if it contains exclusively domains with $n\geq 6$ and pentagonal bubble traps. Figure 1 has this property, except for two pentagonal domains of type $(n,m)=(1,2)$ and one of type (3,1).

Now let us perturb a static configuration by destroying one pentagonal bubble trap. As a result, two of its neighbors, who all had $n\geq 6$, each lose one wall and one neighbor gains a wall [see Fig. 2(b)]. The probability that this neighbor was a hexagon is

$$R_6=\frac{Q_6}{1-Q_5} , \tag{9}$$

since it was a random neighbor, known not to be a pentagon. If it were a hexagon, decrementation would transform it into a pentagon, which then shrinks. When it has shrunk to the size of a bubble trap, it remains in the ensemble as such if none of its five neighbors are bubble traps themselves. This is the case with probability

$$p_0^{(\mathrm{trap})}=(1-Q_5)^5 . \tag{10}$$

If $k\geq 1$ of its neighbors, on the other hand, are also bubble traps, then all $k+1$ of them annihilate with each other and disappear from the ensemble, while their topological deficit $k+1$ is transferred to their neighbors, which are known not to be traps. This happens with probability

$$p_k^{(\mathrm{trap})}=\binom{5}{k}Q_5^k(1-Q_5)^{5-k} . \tag{11}$$

Figure 3 illustrates the case of $k=1$; i.e., two neighbor traps disappear from the ensemble. The case of $k=2$ is rare, and $k>2$ extremely rare, which is good for the consistency of our random-neighbor approximation. More than two pentagonal traps cannot be arranged as neighbors to one pentagon without some of them being neighbors, in conflict with our assumptions. Nevertheless, we keep the small contributions from $k>2$ in our equations, since this yields simpler analytical expressions.

When $k+1$ pentagons disappear from the ensemble and transfer their topological deficit to $k+1$ of their neighbors, known not to be pentagons, b new pentagons are created with probability

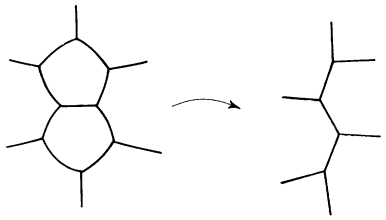

FIG. 3. Two neighbor pentagonal bubble traps disappear, and two of their neighbors lose a neighbor.

$$p_{b;k+1}^{(\text{branch})} = \begin{bmatrix} k+1 \\ b \end{bmatrix} R_6^b (1-R_6)^{k+1-b} . \tag{12}$$

They, for their part, will shrink and either remain in the ensemble as traps or annihilate with one or more other traps. In short, we have a chain reaction at hand. This reaction process, initiated by the destruction of one pentagonal trap and the creation of up to two shrinking pentagons, may be represented diagrammatically as shown in Fig. 4. In Fig. 4 the time axis points downward and a shrinking pentagon is represented by a line. If, at the end of the shrinking process, the pentagon annihilates with one or more traps and creates $b>0$ new shrinking pentagons, this process is represented by a node, out of which comes b new lines. This happens with probability $p_b^{(\text{branch})}$ given below. If, alternatively, the shrinking pentagon remains in the ensemble as a trap or annihilates with other traps without creating new shrinking pentagons, then the line representing it ends with no node at its end. This happens with probability p_0 given below. Such a line is called a *leaf*, while a line connecting two nodes is called a *branch*. The entire graph is called a *tree*, and the process it represents is called a *branching process* [9]:

$$\begin{aligned} p_0^{(\text{branch})} &= p_0^{(\text{trap})} + \sum_{k=1}^{5} p_k^{(\text{trap})} p_{0;k+1}^{(\text{branch})} \\ &= R_6(1-Q_5)^5 + (1-R_6)(1-R_6Q_5)^5 , \end{aligned} \tag{13}$$

$$p_b^{(\text{branch})} = \sum_{k=\max(b-1,1)}^{5} p_k^{(\text{trap})} p_{b;k+1}^{(\text{branch})} \quad \text{for } b>0 .$$

An avalanche of vanishing domains described as a branching process affects P_n and, hence, Q_5 and R_6 and the branching ratios $p_b^{(\text{branch})}$, as the avalanche proceeds. However, if an avalanche affects only a finite number of domains and this number is small compared to the total number in the ensemble, then one may neglect fluctuations in P_n and $p_b^{(\text{branch})}$. If furthermore the ensemble self-organizes under the driving force of avalanches to a statistically stationary state in which P_n and, therefore, $p_k^{(\text{trap})}$, $k=0,1,\ldots,5$, and $p_b^{(\text{branch})}$, $b=0,1,\ldots,6$, remain *constant* within negligible fluctuations, *then* the theory of branching processes yields the asymptotic form of the distribution for the "height" of a tree as measured in number of consecutive branches. This distribution is our theoretical counterpart to the experimental distribution for the duration of avalanches given in [3]. The physical equivalent of one branch, measured, for example, in seconds, can only be determined experimentally, as it was in [2]. But the distribution's asymptotic form is known from the theory of branching processes [9].

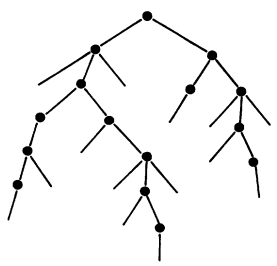

FIG. 4. Tree diagram for branching process. The direction of time is downward.

Using the techniques of the theory of branching processes, we can also find the asymptotic form of the distribution $D(s)$ for the size s of an avalanche; i.e., the number of vanished domains. This is done in Sec. V.

IV. SIMULATION

We have performed computer simulations of the steady-state dynamics described in the previous section. As dynamical variables, we used numbers N_n, $n=5,6,\ldots,$ and M. Here N_n denotes the number of domains in the ensemble with topology n. These numbers were initialized so that the total number of domains, $N\equiv\sum_n N_n$, was large, of order 10^6. Whenever N after a number of avalanches sank below half its initial value, we doubled all the numbers N_n. This choice of range for N strikes a balance between the need for a large ensemble and the need for an ensemble that can be brought into equilibrium with a reasonable number of avalanches and also produce good statistics once it has equilibrated.

Avalanches were initiated by destroying a pentagonal bubble trap—i.e., by decrementing N_5 by 1—and choosing three nonpentagonal neighbors to have their topologies changed: two of them by -1, one of them by $+1$. This was done by first choosing at random three topological numbers n_1, n_2, and n_3, with probability

$$R_n \equiv Q_n/(1-Q_5) = nN_n/(6N-5N_5) , \tag{14}$$

and then decrementing N_{n_1}, N_{n_2}, and N_{n_3} by 1 and incrementing N_{n_1-1}, N_{n_2-1}, and N_{n_3+1} by 1. If either n_1 or n_2 equals 6, then $M=1$ or 2 new pentagons have been created and start shrinking. Otherwise, an avalanche of size 1 was registered. The integer M represents the momentary number of shrinking pentagons in the domain pattern. As long as $M>0$, an avalanche is in progress. We let it progress by reducing M by 1. This represents a shrinking pentagon reaching trap size. This newly formed trap has k neighbor traps with probability $p_k^{(\text{trap})}$ given in Eq. (11). For $k=0$ it remains in the pattern, and we proceed to reduce M by another unit, unless $M=0$, which means the avalanche stops. For $k>0$ we let $k+1$ traps disappear by decrementing N_5 by $k+1$ and transfer their topological deficit to $k+1$ nonpentagonal neighbors. This is done by choosing $k+1$ random integers (n_i), $i=1,2,\ldots,k+1$, larger than 5 with probability R_n and decrementing N_{n_i} by 1, while incrementing N_{n_i-1} by 1. M was simultaneously incremented by b, the number of

numbers n_i that equaled 6.

The number M of shrinking pentagons fluctuates as the avalanche evolves, as just described. When M becomes 0, the avalanche is over, and we register its size—i.e., the total number of pentagons that disappeared—and start another avalanche.

Topologies are always decremented in these avalanches, except in the initial process, when one domain has its topology incremented. The question then is, whether or not this dynamics will drive the system toward a definite distribution (P_n), $n=5,6,\ldots$, that remains static within small fluctuations caused by avalanches that remain small in the "thermodynamical" limit $N\to\infty$. That is, is the system self-organizing, and if so, to which type of state? Will the avalanches be limited in size; i.e., is the stationary state subcritical? Or will, possibly after a transient time, fluctuations as large as the system occur for any value of N; i.e., has the system self-organized into a critical state [4]?

We found that after an initial transient time the values of N_n were constant within small fluctuations. So our simulation indicates that the system self-organizes to a steady state with negligible fluctuations in the thermodynamical limit. Figure 5 shows the relative probabilities (P_n) $n=5,6,\ldots$, as a function of simulation time—i.e., the avalanche number—for two different initial conditions. The solid curves represent, from the bottom up, P_5, P_5+P_6 and $P_5+P_6+P_7$ for initial condition $P_5=P_7=\frac{1}{2}$; $P_6=P_8=P_9=P_{10}=\cdots=0$. The sum $P_5+P_6+P_7+P_8$ and the sums with more terms are at all times indistinguishable from unity in the figure. The dashed curves correspond to initial condition $P_5=P_7=\frac{1}{5000}$, $P_6=\frac{4998}{5000}$, and $P_8=P_9=\cdots=0$. In the simulations yielding these curves, the number of domains

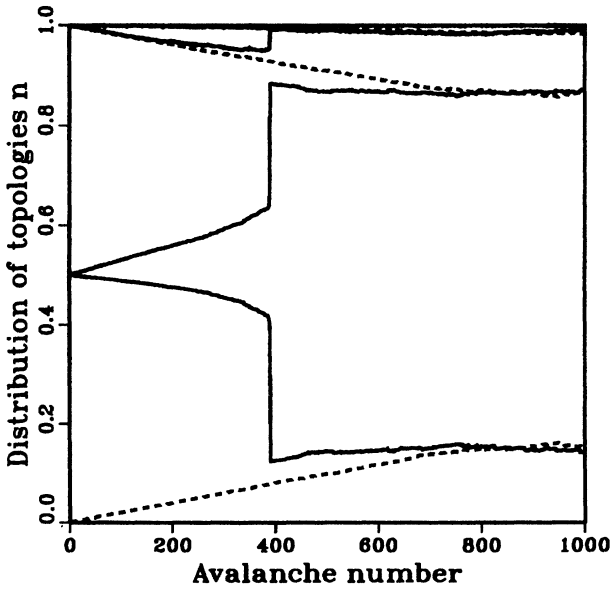

FIG. 5. Probabilities P_n, $n=5,6,7,\ldots$, as a function of simulation time (equal to the avalanche number) for two different initial partitions. From the bottom up, the curves are P_5, P_5+P_6 and $P_5+P_6+P_7$. Sums with more terms are indistinguishable from 1.

was initially 5000 and was doubled whenever it sank below 2500.

The solid curves show P_6 growing gradually from zero until a huge avalanche sweeps through the ensemble and changes its distribution of topologies to a value close to the asymptotic distribution reached after ~ 800 avalanches. The mechanism behind this behavior is easily understood: A high density of isolated pentagonal traps such as the initial one is unrealistic, but also insufficient to keep an avalanche running. That requires a certain density of hexagons, too, because only hexagons can be turned into the new shrinking pentagons required to keep an avalanche running. So, for a while, only small avalanches occur, while P_6 slowly grows as the avalanches produce hexagons. But when P_6 grows beyond a certain value, the high density of pentagons *and* hexagons is supercritical, and a huge avalanche occurs and radically changes the state to one that changes little thereafter.

The gradual, monotonic approach of the dashed curves to their asymptotic values indicates that the system is taken through subcritical states that support only small avalanches. Again, the reason is easily understood: The very low initial density of pentagonal traps makes only very short chain reactions probable. After approximately 800 avalanches, the solid and dashed curves are seen to coincide, essentially. This indicates that the system does indeed self-organize to a unique state under the dynamics we have assumed and simulated. The lack of total coincidence of the curves is fully explained as a finite-size effect in a subcritical state: The initial size of the ensemble of domains was 5000, and it never gets much below 2500 in the simulation. If avalanches are ~ 1 in size, we expect fluctuations of ~ 0.02 on the curves shown, which is what Fig. 5 shows asymptotically.

The subcritical nature of the self-organized state is confirmed by simulation results for the distribution of avalanche sizes, $D(s)$, shown in Fig. 6(a). The data shown in this figure were produced by equilibrizing an initial 10^6 domains through 10^6 avalanches and binning the sizes of the following 10^6 avalanches to obtain $D(s)$. In the figure we see that, for $10<s<100$, $D(s)$ closely follows a straight line with slope $-\frac{3}{2}$, i.e., $D(s)\propto s^{-3/2}$. For larger values of s, however, $D(s)$ falls off faster than this power law. The following section describes how this occurs. For illustration and later use, we give values measured in the same simulation for (P_n), $n=5,6,\ldots$, in Table I and for (p_b), $b=0,1,\ldots,6$, in Table II. Because of small stochastic errors on these numbers, the measured values for (p_b), $b=0,1,\ldots,6$, are not exactly equal to the values one may calculate from the measured values for (P_n), $n=5,6,\ldots$, using the formulas in Sec. III.

V. THEORETICAL RESULTS FOR BRANCHING PROCESSES

The tree structure of the graph in Fig. 4 allows us to write down a recursion relation for the distribution $D(s)$ for the number s of domains that vanish in an avalanche initiated by a shrinking pentagonal domain:

$$D(s')=p_0^{(\text{branch})}\delta_{s',0}+\sum_{k=1}^{5}p_k^{(\text{trap})}\sum_{b=0}^{k+1}p_{b;k+1}^{(\text{branch})}\sum_{s_1=0}^{\infty}\cdots\sum_{s_b=0}^{\infty}\delta_{s'-k-1,s_1+\cdots+s_b}D(s_1)\cdots D(s_b)\ . \tag{15}$$

The total number of domains vanishing in an avalanche initiated by destroying one pentagonal trap is then

$$D^{(\text{total})}(s)=p_{0;2}^{(\text{branch})}\delta_{s,1}+p_{1;2}^{(\text{branch})}D(s-1)+p_{2;2}^{(\text{branch})}\sum_{s_1=0}^{s-1}D(s-1-s_1)D(s_1)\ . \tag{16}$$

But since the asymptotic behavior of $D^{(\text{total})}(s)$ and $D(s)$ for $s\to\infty$ turns out to be the same and that is all we can calculate analytically, we do not distinguish between the two distributions with our notation.

Introducing the generating function

$$\tilde{D}(z)\equiv\sum_{s=0}^{\infty}z^sD(s)\ , \tag{17}$$

the recursion relation Eq. (15) may be written as

$$\tilde{D}=\mathcal{P}(\tilde{D};z)\ , \tag{18}$$

where we have introduced the polynomial

$$\begin{aligned}\mathcal{P}(\tilde{D};z)&\equiv p_0^{(\text{branch})}+z\sum_{k=1}^{5}p_k^{(\text{trap})}z^k\sum_{b=0}^{k+1}p_{b;k+1}^{(\text{branch})}\tilde{D}^b\\&=(1-Q_5)^5+z[1+R_6(\tilde{D}-1)]\\&\quad\times(\{1-Q_5+Q_5z[1+R_6(\tilde{D}-1)]\}^5\\&\quad-(1-Q_5)^5)\ .\end{aligned} \tag{19}$$

Equation (18) is solved by $\tilde{D}(z)$ for such z values that permit a solution. Since the coefficients $D(s)$ in the sum in Eq. (17) are all positive, the localization z_c of the singularity in $\tilde{D}(z)$ closest to the origin is on the real positive axis. For $z>z_c$ the sum in Eq. (17) is divergent. The values for z_c and the corresponding $\tilde{D}_c\equiv\tilde{D}(z_c)$ are found from Eq. (18), supplemented with the critical condition

$$1=\frac{\partial\mathcal{P}}{\partial\tilde{D}}(\tilde{D}_c;z_c)\ . \tag{20}$$

These equations are easily solved numerically.

For $z\approx z_c$, $\tilde{D}\approx\tilde{D}_c$ and expansion of Eq. (18) around $z=z_c$ gives

$$\tilde{D}(z)-\tilde{D}_c\propto\sqrt{z_c-z}\ . \tag{21}$$

From Eq. (17) follows

$$D(s)=\frac{1}{2\pi i}\oint dz\,z^{-s-1}\tilde{D}(z)\ . \tag{22}$$

For $s\to\infty$ this contour integral is saturated by its contribution from a neighborhood of the singular point closest to the origin. Thus Eqs. (21) and (22) yield

$$\begin{aligned}D(s)&\propto\int_{z_c}^{\infty}dx\,x^{-s-1}\sqrt{x-z_c}\quad\text{for } s\to\infty\\&\propto s^{-3/2}z_c^{-s}=s^{-3/2}\exp(-s/s_0)\quad\text{for } s\to\infty\ ,\end{aligned} \tag{23}$$

where we have introduced s_0 by

$$\exp(1/s_0)\equiv z_c\ . \tag{24}$$

When this asymptotic form for $D(s)$ is inserted in Eq. (16), it is seen that $D^{(\text{total})}$ has the same asymptotic form with the same value for s_0. In this form we note that the power $\frac{3}{2}$ on s is a fixed number equal to the mean-field exponent for $D(s)$ for self-organized critical sandpile models [10,11]. This equality is not so surprising, since the mean-field description of the sandpile models can be understood in terms of critical branching processes [10]. In Eq. (23) we also note the exponential damping factor $\exp(-s/s_0)$. Only for $s_0=\infty$ is $D(s)$ without a charac-

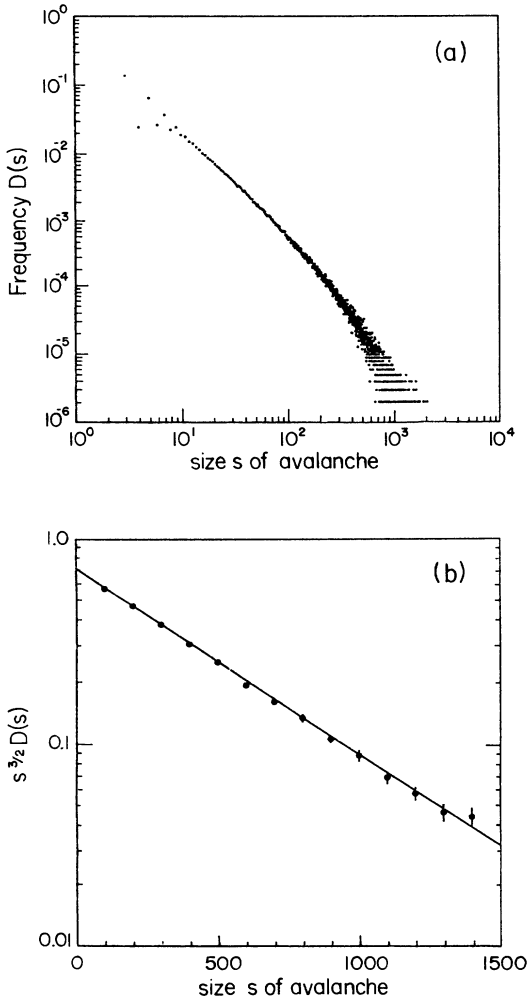

FIG. 6. (a) Relative frequency $D(s)$ of avalanches of size s in simulation of random neighbor model. (b) Simulation result for $s^{3/2}D(s)$ vs s. Results for $s^{3/2}D(s)$ have been averaged over intervals of length 101 centered at s values divisible by 100. The straight line is $s^{3/2}D(s)=0.725\exp(s/s_0)$ with $s_0=475$.

TABLE I. Simulation result for P_n, the probability that a domain has topology n in the steady state. The number of digits given does not reflect the precision of the numbers.

n	5	6	7	8	9	10	11
P_n	0.1535	0.7094	0.1222	0.0135	0.0013	0.0001	0.0000

teristic scale.

Figure 6(b) shows $s^{3/2}D(s)$ plotted against s on semilogarithmic paper. In Fig. 6(b) the data shown in Fig. 6(a) have been multiplied by $s^{3/2}$ and then averaged over bins of width 101 centered at values of s that are integer multiples of 100. The error bars shown for these bin averages were derived from the scatter within bins of $s^{3/2}D(s)$ around its bin average. Consequently, the error bars express not only the scatter of the data around the theoretical curve, but also the variation in this curve across a bin. The contribution from this variation is negligible, because $s^{3/2}D(s)$ is relatively slowly varying. The straight line passing through the data points is the exponential factor in Eq. (23). The value for s_0 was determined numerically from Eqs. (18), (20), and (24) using the values for P_5 and P_6 given in Table I. The overall amplitude in Eq. (23) depends on the detailed properties of the branching process and was fitted to the data points in Fig. 6(b). It is somewhat coincidental that s_0 fits the data so well, since its value is sensitive to the small stochastic errors on the values of P_5 and P_6.

For s_0 large, $z_c \approx 1$ and we can expand Eqs. (18) and (20) in $(z_c, \tilde{D}_c)=(1,1)$ to find

$$\tilde{D}_c - 1 = (z_c - 1)\langle k+1\rangle_{k>0} + (\tilde{D}_c - 1)\langle b\rangle + \tfrac{1}{2}(\tilde{D}_c - 1)^2(\langle b^2\rangle - \langle b\rangle) + (\tilde{D}_c - 1)(z_c - 1)\langle (k+1)^2\rangle_{k>0} , \quad (25)$$

$$1 = \langle b\rangle + (\tilde{D}_c - 1)(\langle b^2\rangle - \langle b\rangle) , \quad (26)$$

where

$$\langle b^l\rangle \equiv \sum_{b=0}^{6} b_l p_b^{(\text{branch})} \quad (27)$$

and

$$\langle (k+1)^l\rangle_{k>0} = \sum_{k=1}^{5} (k+1)^l p_k^{(\text{trap})} . \quad (28)$$

Solving these equations for z_c and inserting the results in Eq. (24), we find

$$s_0 = 2\frac{\langle b^2\rangle - \langle b\rangle}{(1-\langle b\rangle)^2}\langle k+1\rangle_{k>0} + 2\frac{R_6}{1-\langle b\rangle}\langle (k+1)^2\rangle_{k>0} + \text{const} , \quad (29)$$

where const is ~ 1. In this expression for the characteristic number s_0 of domains vanished in an avalanche, the first term is just the characteristic number $2(\langle b^2\rangle - \langle b\rangle)/(1-\langle b\rangle)^2$ of branches and leaves in the branching tree in Fig. 4 *times* the average number $\langle k+1\rangle_{k>0}$ of domains that vanish at the end of a branch or leaf. The second term in Eq. (29) is the result of a positive correlation between fluctuations in the size of a tree and fluctuations in the number of domains vanishing at a node.

The branching process is *critical* if $s_0 = \infty$, which is the case for $\langle b\rangle = 1$. We can easily understand why criticality corresponds to $\langle b\rangle = 1$: A shrinking pentagon, represented as a leaf or a branch in Fig. 4, will on the average branch to $\langle b\rangle$ new leaves and branches, representing shrinking pentagons. When one shrinking pentagon on the average turns into exactly one shrinking pentagon, the branching process just goes on, with no inherent scale in it. For $\langle b\rangle > 1$ the average number of branches grows as a result of branchings, and the process is a runaway, supercritical process, like the 396th avalanche in Fig. 5. For $\langle b\rangle < 1$ the average number of branches decreases as a result of branchings, and the process is subcritical and dies out after a finite number of branchings like the processes plotted in Fig. 6. Using the simulation results given in Table II, we find

$$\langle b\rangle = 0.926\ldots , \quad (30)$$

i.e., the branching process we have simulated is not critical. Since there is no assumption or mechanism in our model that assures $\langle b\rangle = 1$, it is maybe not so surprising that it is not critical. On the other hand, self-organized critical systems exist [4], and so we are induced to reflect on what it is that makes a model with self-organization critical. In the case considered here, a conservation law for the average number of shrinking pentagons, enforced at each node of the tree diagram for the branching process, would clearly do the job. But there is no good reason the model should contain such a conservation law.

The theory for random branching processes gives us the asymptotic behavior for the distribution of lifetimes in an entirely similar way [9]:

$$D(T) \propto T^{-2}\exp(-T/T_0) . \quad (31)$$

TABLE II. Simulation result for p_b, the probability that a shrinking pentagon causes the creation of b shrinking pentagons, when it reaches trap size. The number of digits given does not reflect the precision of the numbers.

b	0	1	2	3	4	5	6
p_b	0.5181	0.1201	0.2871	0.0669	0.0073	0.0004	0.0000

VI. COMPARISON WITH EXPERIMENT

We do not expect that the model developed in the previous sections is a quantitatively precise dynamical model for the topological avalanches studied by Babcock, Seshadri, and Westervelt. Too many simplifications and idealizations were introduced for that to be possible. But we may expect it to reproduce gross features correctly, such as the asymptotic forms given in Eqs. (23) and (31), power laws times exponential damping factors. In particular, we expect the mean-field exponents in $s^{-3/2}$ and t^{-2} to be good approximations, since they are consequences of the random-neighbor approximation, and *that* approximation was shown to be quantitatively correct for two-dimensional domain patterns in [5].

Figures 7 and 8 show semilogarithmic plots of the experimental data from [3] with the power factors divided out. The straight lines in these figures are the results of χ^2 fits of Eqs. (23) and (31) to the data points shown as solid circles. The separation of the data into asymptotic data (solid circles) and nonasymptotic data (open circles) was done by varying the point of separation and choosing the separation that maximized the χ^2 level.

Clearly, the χ^2 levels obtained for these fits are unrealistically large. Their values signal either that the error bars given are too large to be of purely stochastic origin or that the data are correlated. The latter possibility is ruled out on theoretical grounds by the assumption of steady-state dynamics and the random-neighbor description. The former possibility would result from binning the experimental data, using their root-mean-square deviation within a bin as an error bar on the bin average. The mean square deviation resulting from this procedure is the *sum* of the stochastic variance around its average *and* the variance of that average across the bin. Since $D(s)$ and $D(T)$ are fairly rapidly varying functions, the last contribution is significant. The experimental values for $D(s)$ and $D(T)$ *were* binned in [2], though we do not know precisely how. Whatever the reason for the size of the error bars, we can reduce them by a factor 2 and still fit the data with χ^2 levels larger than 70%.

Comparing the experimental value $s_0 \simeq 29$ shown in Fig. 7 with our model's value $s_0 = 477$, the difference, a factor 16, is not in accord with our repeated reference to the random-neighbor approximation as being reliable. This approximation *was* found to give reliable results for distributions of domain areas and topologies in [5]. However, as with all approximation, some quantities are approximated better than others, and the expression for s_0 in Eq. (29) shows that s_0 is particularly sensitive to errors on $\langle b \rangle$. Calculation of s_0 from the exact expression Eq. (24) shows that a 23% reduction in Q_5 relatively to its value taken from Table I suffices to reduce s_0 from 477 to its experimental value 29.

We finally remark that there is no way to relate s_0 and T_0 theoretically for dimensional reasons. T_0 simply sets the scale of time in the experiment.

VII. DISCUSSION AND CONCLUSIONS

We have considered the possibility of changing the model presented above with an eye on the experimental results in order to reproduce them better. According to Eq. (29), what we need in order to decrease our values for s_0 and T_0 is to shift the weights of $p_b^{(\text{branch})}$ and $p_k^{(\text{trap})}$ toward the lower values for b and k—i.e., we need "less branching and less vanishing" per pentagon that shrinks to trap size. This we cannot obtain within the random-neighbor approximation, it seems. The random-neighbor ansatz fixes the relative probabilities with which topologies of neighbor domains are chosen and leaves us at most with a choice of the *number* of neighbors affected: Instead of decrementing the topologies of $k+1$ nonpentagonal neighbors, when $k+1$ traps vanish, we may

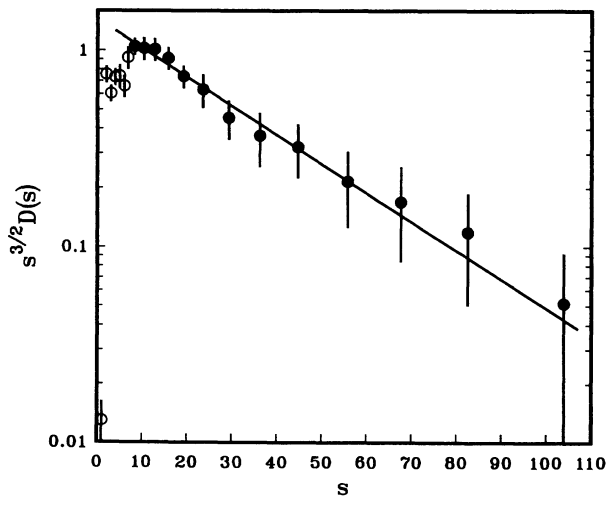

FIG. 7. Experimental results from [3] for $s^{3/2}D(s)$ vs s. The straight line is a least-squares fit of the functional form in Eq. (23) to the experimental data plotted as solid circles. The χ^2 level for the fit is 99.8%. It has $s_0 \simeq 29$, with s_0 defined in Eq. (23).

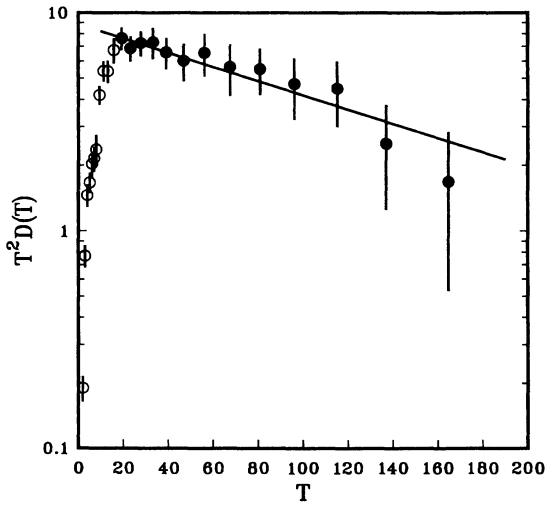

FIG. 8. Experimental results from [3] for $T^2D(T)$ vs T. The straight line is a least-squares fit of the functional form in Eq. (31) to the experimental data plotted as solid circles. The χ^2 level for the fit is 99.7%, with $T_0 \simeq 133$ sec.

choose to decrement a larger number, while incrementing another number so that Euler's law is still respected. But such a change causes *more* domains to vanish per shrinking pentagon and *more* branching to occur. Any such change away from the minimal solution we have used so far is a change in the wrong direction. Simulations with procedures changed this way yield supercritical dynamics: avalanches never stop.

Revisiting Aboav's law [Eq. (3)], which we ignored with the random-neighbor approximation, we note that it expresses a *negative* correlation between topologies of neighbor domains: Domains with lower topological numbers have neighbors with higher topological numbers on the average and vice versa. Aboav's law is phenomenological in origin [8], but various derivations of approximate forms of the law are based on local enforcement of Euler's law [Eq. (5)]: Typically, a pentagon will have a heptagonal nearest neighbor and vice versa [6]. So the probability Q_5 that a neighbor to a shrinking pentagon is a pentagonal trap is really smaller than $\frac{5}{6}P_5$. This is what we need: With local enforcement of Euler's law—which by the way is borne out in Fig. 1—pentagonal traps can be present in the ensemble in larger proportions and yet be less accessible to other pentagons than is possible within the random-neighbor approximation. That causes less domains to vanish and suppresses branching, since an increase in P_5 decreases P_6 because P_n, $n \geq 7$, must be increased with P_5 according to Euler's law. Simulations with *ad hoc* suppression of Q_5 relatively to $\frac{5}{6}P_5$ confirms this picture. But since we do not have a systematic way to improve the random-neighbor approximation with nearest-neighbor correlations, we stop here with this understanding of the source of our errors.

Irrespective of the details of our model, the sloping straight lines fitting the data in Figs. 7 and 8 clearly demonstrate that the avalanches studied belong to a *subcritical* self-organized state.

ACKNOWLEDGMENTS

P. B. thanks Ken Babcock and Robert Westervelt for discussions of their experimental results. P. B.'s research was supported by the Division of Materials Science, U.S. DOE, under Contract No. DE-AC02-76CH00016. H. F. thanks the Physics Department at Brookhaven National Laboratory for hospitality while this work was commenced.

[1] K. L. Babcock and R. M. Westervelt, Phys. Rev. A **40**, 2022 (1989).
[2] K. L. Babcock, R. Seshadri, and R. M. Westervelt, Phys. Rev. A **41**, 1952 (1990).
[3] K. L. Babcock and R. M. Westervelt, Phys. Rev. Lett. **64**, 2168 (1990).
[4] P. Bak, C. Tang, and K. Wiesenfeld, Phys. Rev. Lett. **59**, 381 (1987); Phys. Rev. A **38**, 364 (1988).
[5] H. Flyvbjerg and C. Jeppesen, Phys. Scr. **T38**, 49 (1991).
[6] D. Wearie and N. River, Contemp. Phys. **25**, 59 (1984).
[7] J. von Neumann, in *Metal Interfaces,* edited by C. Herring (American Society for Metals, Cleveland, OH, 1952), p. 108; W. W. Mullins, J. Appl. Phys. **27**, 900 (1956).
[8] D. A. Aboav, Metallography **13**, 43 (1980).
[9] T. E. Harris, *The Theory of Branching Processes* (Springer, Berlin, 1963).
[10] P. Alstrøm, Phys. Rev. A **38**, 4905 (1988).
[11] D. Dhar and S. N. Majumdar, J. Phys. A **23**, 4333 (1990).